International Journal of Heat and Mass Transfer 192 (2022) 122894

Contents lists available at ScienceDirect

International Journal of Heat and Mass Transfer

journal homepage: www.elsevier.com/locate/hmt

Flow condensation heat transfer and pressure drop of R134a alternative refrigerants R513A and R450A in 0.95-mm diameter minichannels

Jordan A. Morrow, Melanie M. Derby*

3002 Rathbone Hall, 1701B Platt St., Alan Levin Department of Mechanical and Nuclear Engineering, Kansas State University, Manhattan, KS, USA

ARTICLE INFO

Article history:
Received 21 January 2022
Revised 16 March 2022
Accepted 1 April 2022
Available online 21 April 2022

Keywords:
Condensation
Low global warming potential
Low GWP
Alternative refrigerant
Two-phase flow

ABSTRACT

Due to the Kigali amendment to the Montreal Protocol, refrigerants such as R134a are targeted for phase-down or phaseout due to their global warming potential (GWP) and lower GWP refrigerants are being considered to replace R134a. Since the condenser is typically responsible for 50% of the charge of a refrigeration system, it is vital to have a fundamental understanding of the flow condensation heat transfer performance of low GWP refrigerants such as R513A and R450A. Experimental flow condensation heat transfer coefficient data are reported for R134a, R513A, and R450A in seven parallel 0.95 mm diameter mini-channels for a range of mass fluxes (i.e., 200 – 500 kg/m^{2}s) and qualities (i.e., 0.2 – 0.8) at a saturation temperature of 40 °C. The heat transfer coefficient uncertainties for all experiments were ± 6.3 – 21.2%, with an average of ± 9.8%. Condensation heat transfer coefficients for R134a, R513A, and R450A all increased with increasing mass flux and quality. R513A condensation heat transfer coefficients were 2.6 – 25.6% lower than R134a heat transfer coefficients and pressure drops were 4.5 – 14.0% lower than R134a pressure drops. R450A heat transfer coefficients were 2.4% higher than R134a at higher mass fluxes and qualities and up to 11.7% lower than R134a at lower mass fluxes than R134a heat transfer coefficients; R450A pressure drop were comparable to R134a pressure drop (i.e., 5.0% higher to 9.5% lower). The data were compared to three condensation correlations – Shah (2016), Kim and Mudawar (2013), and Cavallini et al. (2011); the data were predicted with mean average errors of 23.4%, 15.9%, and 23.4%, respectively.

1. Introduction

In 1987, the Montreal Protocol initiated a plan for phasing out substances that had an ozone depletion potential greater than zero – including refrigerants (i.e., chlorofluorocarbons); these fluids were phased out and replaced with hydrofluorocarbons (HCFCs) and hydrofluorocarbons (HFCs), with most HCFCs being phased out later [1]. The F-Gas regulations in the European Union in 2015 and the Kigali Amendment to the Montreal Protocol in 2016 specified timelines for phasing out refrigerants that have a high global warming potential (GWP); these phase outs are in progress and will continue for years to come [2]. Low GWP alternative refrigerants include a new category of refrigerants called hydrofluoroolefins, or HFOs, which have GWPs less than 10 [3]. Other alternatives for high GWP refrigerants are natural refrigerants (e.g., propane and ammonia) and HFC/HFO mixtures. Natural refrigerants all boast extremely low GWP values (e.g., less than 10) [4], while HFC/HFO mixture refrigerants have GWP values that generally range between 100 and 1000 [2,5].

The challenges that come with this transition to lower GWP refrigerants are safety, performance, and cost concerns. Natural refrigerants offer low GWPs but are often flammable, toxic, or both, or they run at very high pressures which increases costs [4,6]. HFOs are mildly flammable, very costly, and may show performance reductions [3,7]. HFC/HFO mixtures have higher GWP values (compared to other alternatives) and some are mildly flammable; however, they tend to show less performance reductions than HFOs compared to incumbent refrigerants [5]. Two promising non-toxic and non-flammable (i.e., A1) R134a alternative refrigerants are R513A (GWP = 573) and R450A (GWP = 547).

In order to minimize charge, it is important to reduce the size of the condenser, which is typically the largest component of the refrigeration system [8]. One option is to move to mini- and microchannel tubes, as heat transfer performance increases with the decreasing diameter [9–11]. Some of these alternative refrigerants have been well characterized, but many of these alternative refrigerants still lack data quantifying condensation heat transfer performance. Morrow et al. [12] compiled a database of 6505 flow

* Corresponding author.
E-mail address: derbym@ksu.edu (M.M. Derby).

https://doi.org/10.1016/j.ijheatmasstransfer.2022.122894
0017-9310/

Nomenclature

A	area, m
A_s	surface area, m
c_p	specific heat, J/kg K
D	diameter, m
$\frac{dT}{dy}$	temperature gradient in the y direction, K/m
G	mass flux, kg/m^{2}s
h	heat transfer coefficient, W/m^{2}K
i_{lv}	latent heat of vaporization, J/kg
I	enthalpy, J/kg
k	thermal conductivity, W/m K
$\dot{m}$	mass flow rate, kg/s
q''	heat flux, W/m^2
$\dot{Q}$	heat transfer, W
T	temperature,°C
x	quality
y	distance in the vertical direction, m

Non-dimensional numbers

Nu	Nusselt number
Pr	Prandtl number
Re	Reynolds number

Greek

μ	viscosity, Pa s
ρ	density, kg/m^3
ω	uncertainty

Subscripts

A, B, C	pertaining to location A, B, C
block	pertaining to the heat flux block
ch	channel
cond	condensation
cu	copper
fluid	pertaining to the fluid
header	pertaining to the header
in	inlet
l	liquid
out	outlet
pre	precondenser
ref	refrigerant
sp	single-phase
tc	thermocouple
v	vapor
vo	vapor only
wall	pertaining to the wall
water	pertaining to water

condensation heat transfer data points; of these, there were only 58 and 106 data points for R513A and R450A, respectively. There are several correlations that are widely used and accepted as being good predictors of heat transfer coefficients; however, most of these correlations were developed with few or no low GWP refrigerant alternatives [12].

R513A was investigated as a potential drop-in replacement for R134a in different systems including small scale vapor compression systems and mobile air conditioning units. Studies showed that R513A typically has a modest reduction in coefficient of performance (COP) (i.e., up to 9%) compared to R134a [13–21], although a few studies found R513A to have a higher COP [2,22]. Sjoholm and Ma [16] and Yildiz and Yilirim [23] showed R513A to have higher COP than R134a at low evaporator temperatures (i.e., less than 0 °C) and freezer conditions, suggesting its potential for use in freezer applications. R513A performed with a similar cooling capacity to R134a [2,13–15,18,19,22], though Sun et al. [20] saw a 12% reduction in cooling capacity.

R450A was investigated as an R134a replacement in different vapor compression systems. Experimentally, R450A has similar COP (up to 4% reduction) compared to R134a [13,14,17,18,24,25]. The cooling capacity of R450A is considerably lower than R134a, however– somewhere between 6-23% [13,14,17,18,24] due to the R1234ze(E) in R450A. R450A was also found to be a potential drop-in replacement for R134a [26], including as a potential alternative for adsorption systems [27].

Condensation heat transfer coefficient data for R513A are limited (Table 1). Much of the data were investigated in mini-channels (i.e., 0.72 – 2.5 mm [28–30]), while some were investigated in smaller conventional-sized tubes (i.e., 3.4 – 9.52 mm [31,32]). R513A heat transfer coefficients were investigated in smooth and microfin tubes, and in single channel [30–32] and multi-channel test sections [28,29]. R513A increased with increasing quality and mass flux in five studies [28–32]. Higher mass fluxes present higher slopes because of the higher convective effect [30].

Lopez-Belchi [28] investigated R513A, R1234yf, and R134a in 1.16-mm diameter multiport channels. R513A heat transfer coefficients were about 10% lower than R134a, but R513A pressure drop was also about 10% lower. Morrow et al. [29] investigated R513A and R134a in 0.72 mm-diameter multiport channels. R513A heat transfer coefficients were similar to R134a. Diani et al. [31] investigated R513A in a 3.5 mm diameter smooth tube and 3.4 mm diameter microfin tube. The microfin tube showed greatest enhancement of heat transfer performance at lower mass fluxes (i.e., less than 400 kg/m^{2}s). Diani and Rossetto [30] investigated R513A in a 2.5 mm smooth tube and a 2.4 mm microfin tube and compared the data to R134a. R513A heat transfer coefficients were compared to R134a in the microfin tube and found to be about 10% lower than R134a, with greater differences at higher mass fluxes and qualities. R134a had higher performance due to its larger liquid thermal conductivity and lower vapor density. The lower vapor density means R134a has higher velocities at the same mass flux, meaning a greater convective effect. R134a had about 10% higher pressure drop than R513A. At a lower saturation temperature, the condensation heat transfer coefficients were higher because of the lower vapor density [30].

Data on R450A condensation heat transfer coefficients are very limited (Table 2). Jacob et al. [33] conducted an experimental investigation of R450A in a 4.7-mm inner diameter smooth tube at mass fluxes of 100 to 550 kg/m^{2}s, saturation temperatures of 45 and 55 °C, and the full range of qualities. R450A heat transfer coefficients were found to increase with increasing mass flux and quality. R450A was compared to R134a and found to have lower heat transfer coefficients, but no more than 5% different at higher qualities; however, R450A also showed an average of 8% higher pressure drop than R134a. Liu et al. [34] presented simulated heat transfer coefficient data of R450A using tube diameters of 1 and 2 mm. At mass fluxes of 400, 600, and 800 kg/m^{2}s, R134a showed 7.5–16.3% higher heat transfer coefficients than R450A. With heat transfer coefficients up to 15% lower than R134a and higher pressure drops than R134a, systems using R450A would need additional modifications to account for the performance degradations.

R513A and R450A are potential lower GWP, A1 alternatives to R134a, but there are limited data. The research objectives of this paper are to experimentally measure flow condensation heat transfer coefficients and pressure drops of R513A and R450A in 0.95 mm square channels and compare the data to R134a.

2. Experimental apparatus

A vapor compression cycle was designed to measure condensation heat transfer coefficients for R134a and its alternatives (Fig. 1),

Table 1
Summary of R513A heat transfer coefficient literature.

Paper	Diameter [mm]	Sat temp [°C]	Mass flux [kg/m^{2}s]	HTC	Pressure drop
Morrow et al. (2018)	0.72 square multichannel	40	300, 400, 500	Similar to R134a	
Lopez-Belchi et al. (2019)	1.16 square multichannel	40	470, 710	10% lower than R134a	10% lower than R134a
Diani et al. (2020)	3.5 smooth, 3.4 microfin	30, 40	100 – 1000	microfin tube had greater enhancement at low mass flux	
Diani and Rossetto (2020)	2.5 smooth, 2.4 microfin	30, 40	300 - 1000	10% lower than R134a	10% lower than R134a
Karageorgis et al. (2021)	9.52 OD microfin	35	100 - 440	10% higher than R134a	

Table 2
Summary of R450A heat transfer coefficient literature

Paper	Diameter [mm]	Sat temp [°C]	Mass flux [kg/m^{2}s]	HTC	Pressure drop
Jacob et al. (2019)	4.7	40	100–550	5% lower than R134a	8% higher than R134a
Liu et al. (2021)	1, 2	40	400, 600, 800	7.5–16.3% lower than R134a	

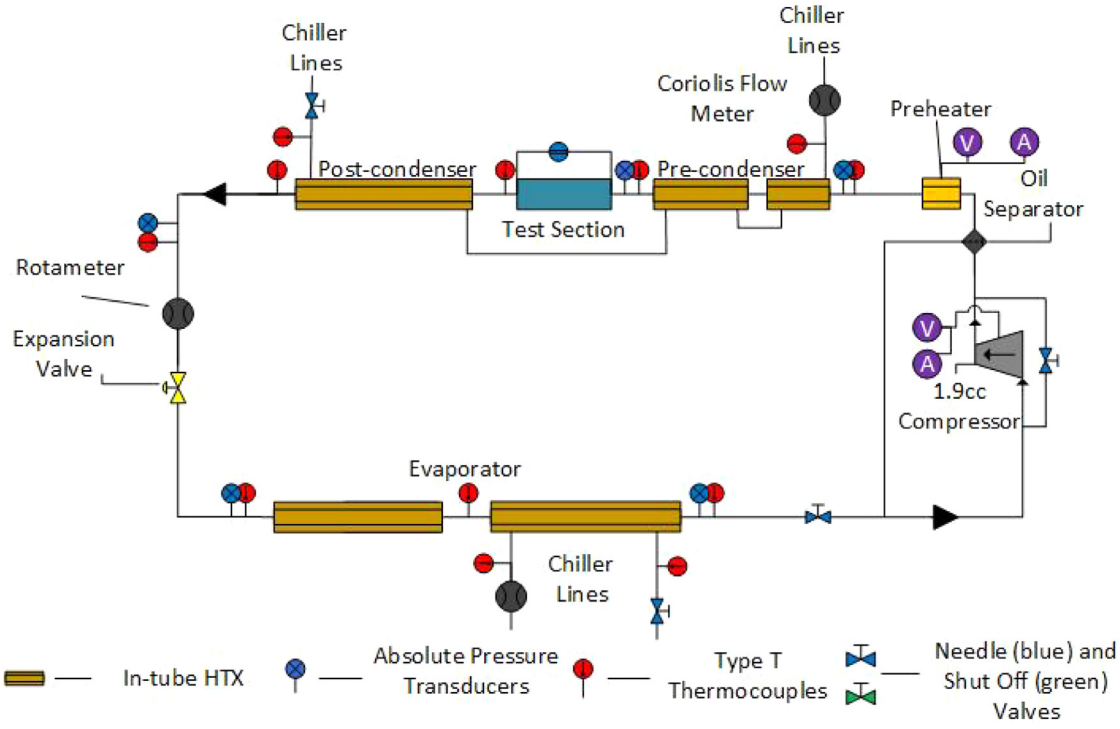

Fig. 1. Schematic of vapor compression cycle designed for R134a and its alternatives.

and a brief description of the flow path follows. The refrigerant leaves the compressor (Aspen 19-24-1101) as a high-pressure vapor that passes through an oil separator (Temprite Model 320), separating out any oil that left the compressor; the oil returns to the low-pressure side of the system via capillary tube. Previous experiments using a Coriolis flow meter to measure refrigerant density showed less than 1% difference in expected refrigerant density, indicating that the oil circulating through the system is negligible.

After exiting the oil separator, the refrigerant flows by an in-flow cartridge heater (Watlow FIREROD 1902) used to heat the refrigerant to a vapor with a superheat greater than 5 °C to set the state of the refrigerant prior to entering the condenser section. After superheating, the refrigerant enters the pre-condenser consisting of two tube-in-tube heat exchangers in series, in which refrigerant flows through the inner tube and water flows through the annulus in a counter-flow configuration. A recirculating chiller (Neslab ThermoFlex 2500) with a valve controls the water flow and temperature, and a Coriolis flow meter (Micro Motion 5700) measures the water mass flow rate. Type T thermocouples (Omega TMQSS-116U-6) measure the inlet and outlet temperatures of the water. The temperature (Omega TMQSS-116U-6) and pressure (Omega PX309-300A5V) of the refrigerant are measured at the inlet and outlet of the pre-condenser section. Following the pre-condenser, the refrigerant enters a copper test section (Fig. 2) with seven 0.95 mm parallel channels, as described in Section 2.1. The pressure drop is measured across the test section using a differential pressure transducer (Setra 2301030PD2F2DA). The refrigerant flow enters the test section from includes a Swagelok cross fitting (SS-400-4), a Swagelok elbow fitting (SS-400-9), and a Swagelok NPT straight fitting (SS-400-5-4). The refrigerant flow leaves the test section through the same connections is reverse order. The pressure drop is measured between the two cross fittings. The refrigerant leaves the test section and passes through the post-condenser, two tube-in-tube heat exchangers that fully subcool the refrigerant.

The high-pressure, subcooled liquid refrigerant enters a four-tube rotameter (Omega FL-4SB-40C-40ST-39ST-39G-PTFE) that measures the volumetric flow rate and, therefore, mass flow rate, of the refrigerant using the calibrations conducted for R134a, R513A, and R450A. Only the smallest rotameter tube was used for these experiments. Immediately after exiting the rotameter, the refrigerant passes through a manual expansion valve (Swagelok SS-

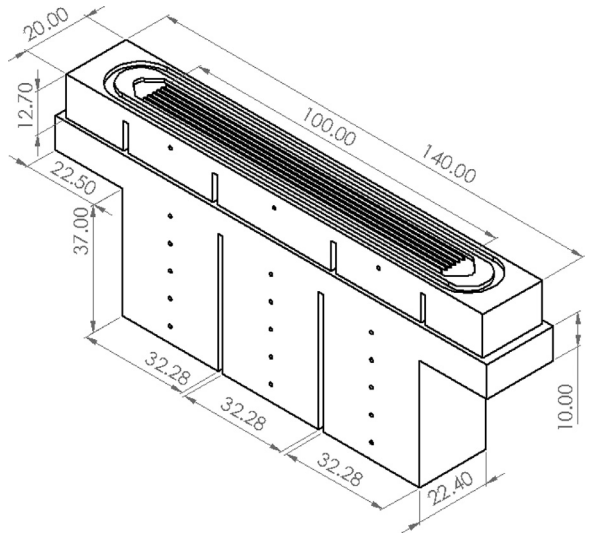

Fig. 2. Schematic of test section assembly showing square channel test coupon and three segment heat flux block.

SS4) and subsequently the low-pressure, liquid-vapor mixture refrigerant flows through to a two tube-in-tube heat exchanger evaporator and returns to the compressor.

2.1. Test Section

The test section is a machined coupon and heat flux block made from oxygen-free copper as discussed in Derby et al. [35]. The coupon consists of seven parallel channels, each with a height of 0.98 mm and a width of 0.93 mm, resulting in a hydraulic diameter of 0.95 mm. The wall thickness between each channel is 0.5 mm and the length of the test section is 100 mm. The coupon contains an inlet and outlet header. Based on simulations conducted previously by Derby et al. [35,36], the heat transfer coefficient to calculate the heat transfer rate in the inlet and outlet headers equals the heat transfer coefficient of the adjacent segment (i.e., the inlet header is assumed to have the same heat transfer coefficient as the first segment, and the outlet header is assumed to have the same heat transfer coefficient as the third segment).

The heat flux block is used to measure to heat flux leaving the bottom surface of the coupon. The heat flux block is comprised of three segments to reduce axial conduction [36]. Each segment consists of five 1 mm-diameter thermocouples, the first 8 mm from the top surface of the heat flux block and each one 8 mm lower in the y-axis. These type T thermocouples (Omega TJ36-CPSS-040U-6) aligned to the center of each segment measure the heat flux leaving the refrigerant. One the middle segment is used for measuring heat transfer coefficients due to the entrance and exit effects of the test section. Wall temperature is measured by a thermocouple in the coupon located 3 mm from the channel bottom. Thermal paste (Arctic Silver 5) is used between the coupon and the block to reduce the contact resistance. A stainless-steel cooling block with a serpentine channel below the heat flux block is used to have a constant heat flux boundary condition for cooling the refrigerant. A layer of thermal paste (Arctic Silver 5) is used between the copper block and the cooling block. The test section is clamped together using six bolts.

2.2. Data reduction

To validate the experimental apparatus, single-phase experiments included energy balances and single-phase Nusselt numbers for R134a, R513A, and R450A. For single-phase experiments, the pre-condenser sub-cools the refrigerant entering the test section by at least 5 °C. The refrigerant is then cooled at least 10°C across the test section for each experiment. The heat transfer rate, $\dot{Q}_{ref}$, leaving the refrigerant across the test section is calculated by

$$\dot{Q}_{ref} = \dot{m}_{ref} c_{p,ref} (T_{in} - T_{out}) \tag{1}$$

where $\dot{m}_{ref}$ is the refrigerant mass flow rate, $c_{p,ref}$ is the specific heat capacity of the refrigerant, T_{in} is the temperature of the refrigerant entering the test section, and T_{out} is the temperature of the refrigerant leaving the test section. The heat entering the heat flux block is calculated from the thermocouple measurements and Fourier's. The total block heat transfer rate is calculated as

$$\dot{Q}_{block} = \dot{Q}_{header,in} + \dot{Q}_1 + \dot{Q}_2 + \dot{Q}_3 + \dot{Q}_{header,out} \tag{2}$$

where $\dot{Q}_i$ is the heat transfer rate in each block segment, $\dot{Q}_{header,in}$ is the heat transfer rate in the inlet header of the test section, and $\dot{Q}_{header,out}$ is the heat transfer rate in the outlet header of the test section. The heat transfer rate in each block segment is calculated by

$$\dot{Q}_i = q''_{block} A_{block} \tag{3}$$

where q''_{block} is the heat flux through each block segment and A_{block} is the cross-sectional area of the block's corresponding segment. The heat flux through each block is calculated using Fourier's Law,

$$q''_{block} = -k_{cu} \frac{dT}{dy} \tag{4}$$

where k_{cu} is the thermal conductivity of copper and $\frac{dT}{dy}$ is the temperature gradient in the vertical y axis of each block segment. The temperature gradient is measured for each segment using a linear regression of the form

$$\frac{dT}{dy} = \frac{\sum^{(y_i - \bar{y})} \left(T_i - \bar{T}\right)}{\sum^{(y_i - \bar{y})^2}} \tag{5}$$

where y_i is the distance in the y-axis vertically down of the ith thermocouple from the top of the heat flux block, T_i is the measured temperature of the ith thermocouple, $\bar{y}$ is the average distance in the y-axis vertically down, and $\bar{T}$ is the average measured temperature of the segment. The heat loss in the headers was modeled by Derby et al. [35] and calculated as

$$\dot{Q}_{header} = h_{header} A_{header} \left(T_{wall} - T_{fluid}\right) \tag{6}$$

where h_{header} is the header heat transfer coefficient, A_{header} is the header area, T_{wall} is the assumed header wall temperature, and T_{fluid} is the assumed refrigerant temperature in the header. The header heat transfer coefficients and fluid-wall temperature differences were found to be equal to the heat transfer coefficients and fluid-wall temperature differences of the corresponding segments, i.e., the first segment for the inlet and the third segment for the outlet. The header area was measured as 6E-5 m^2 [36,37].

The single-phase heat transfer coefficient is calculated by

$$h_{sp} = \frac{q''_{ch}}{T_{fluid} - T_{wall}} \tag{7}$$

where q''_{ch} is the heat flux of the test section channel, T_{fluid} is the temperature of the refrigerant, and T_{wall} is the temperature of the channel wall. The fluid temperature is the average of the inlet and outlet measured fluid temperature since the heat transfer coefficient is calculated from the center of the channel. The heat flux in the channel is calculated from the energy balance between the heat leaving the test section channel segment and the corresponding block segment:

$$q''_{ch} A_{s,ch} = q''_{block} A_{block} \tag{8}$$

where $A_{s,ch}$ is the surface area of the test section channel's segment. The thermocouple measuring the wall temperature is 3 mm below the surface, so the wall temperature is extrapolated using the wall thermocouple plus the five thermocouples used to calculate the heat flux in the block. The refrigerant temperature is the average of the inlet and outlet refrigerant temperatures of the test section. The refrigerant Nusselt number is

$$Nu = \frac{hD}{k_{l,ref}} \tag{9}$$

where h is the second segment single phase heat transfer coefficient, D is the hydraulic diameter of the test section channel, and $k_{l,ref}$ is the refrigerant liquid thermal conductivity at the second segment of the test section. Properties were calculated using the refrigerant fluid temperature, which is the average of the inlet and outlet temperature.

The condensation heat transfer coefficient is calculated by

$$h_{cond} = \frac{q''_{ch}}{T_{fluid} - T_{wall}}. \tag{10}$$

The fluid temperature of two-phase condensation is calculated as the saturation temperature for azeotropic fluids (i.e., R134a, and R513A) and the bulk fluid temperature for zeotropic fluids (i.e., R450A). Because of the temperature glide of R450A across the liquid-vapor region, the bulk fluid temperature is a function of pressure and quality. In two-phase flows, the first and third segments are influenced by entrance and exit effects; therefore, the only segment used for measuring refrigerant condensation heat transfer coefficients is the middle segment. A linear pressure drop across the test section is assumed for calculating the fluid pressure used for calculating fluid temperature; the fluid pressure for calculating the heat transfer coefficient is the average of the inlet and outlet pressure

In a similar manner as the single-phase experiments, in two-phase experiments, an energy balance beginning at the entrance of the preheater is used to calculate each segments' quality. The total water side heat transfer is calculated using

$$\dot{Q}_{pre} = \dot{m}_{water} c_{p,water} \left(T_{water,out} - T_{water,in}\right) \tag{11}$$

where $\dot{m}_{water}$ is the mass flow rate of the preheater annulus water flow, $c_{p,water}$is the specific heat capacity of water, and $T_{water,in}$ and $T_{water,out}$ are the measured water temperatures at the inlet and outlet of the preheater, respectively. Since the refrigerant enters the preheater as a superheated vapor, the enthalpy of the refrigerant is found from the temperature and pressure at the inlet of the preheater. The enthalpy at the exit of the preheater, or the inlet of the test section, is found by

$$i_{in} = i_{pre} - \frac{\dot{Q}_{pre}}{\dot{m}_{ref}} \tag{12}$$

where i_{pre} is the enthalpy of the superheated vapor at the inlet of the precondenser. The heat loss in the headers for two-phase flow was also modeled by Derby et al. [35] and calculated as

$$\dot{Q}_{header} = h_{header} A_{header} \left(T_{wall} - T_{fluid}\right) \tag{13}$$

where h_{header} is the header heat transfer coefficient, A_{header} is the header area, T_{wall} is the assumed header wall temperature, and T_{fluid} is the assumed refrigerant temperature in the header. The header heat transfer coefficients and fluid-wall temperature differences were found to be equal to the heat transfer coefficients and fluid-wall temperature differences of the corresponding segments, i.e., the first segment for the inlet and the third segment for the outlet. The enthalpy after the inlet header is calculated from the equation

$$\dot{Q}_{header,in} = \dot{m}_{ref} \left(i_{in} - i_{header,in}\right) \tag{14}$$

where $i_{header,in}$ is the enthalpy after the inlet header, and $\dot{Q}_{header,in}$ is calculated from Eq. (6). The enthalpy of the point after the first block segment is calculated using the equation

$$\dot{Q}_1 = \dot{m}_{ref} \left(i_{header,in} - i_A\right) \tag{15}$$

where $\dot{Q}_1$ is the heat transfer through the first block segment and i_A is the enthalpy after the first block's segment. The enthalpy at the center of the first block segment is calculated by the average between the enthalpy at the beginning and end of the segment:

$$i_1 = \frac{i_{header,in} + i_A}{2} \tag{16}$$

The enthalpy in the middle of segments 2 and 3 are calculated in a similar fashion using energy balances.

2.3. Experimental uncertainties

Experimental uncertainties were calculated using a propagation of uncertainty analysis [38]. The heat transfer coefficient uncertainty was calculated as

$$\omega_h = \sqrt{\begin{array}{l}\left(\frac{\partial h}{\partial q''_{block}}\right)^2 \omega^2_{q''_{block}} + \left(\frac{\partial h}{\partial A_{block}}\right)^2 \omega^2_{A_{block}} + \left(\frac{\partial h}{\partial A_{ch}}\right)^2 \omega^2_{A_{ch}} \\ + \left(\frac{\partial h}{\partial T_{fluid}}\right)^2 \omega^2_{T_{fluid}} + \left(\frac{\partial h}{\partial T_{wall}}\right)^2 \omega^2_{T_{wall}}\end{array}} \tag{17}$$

where ω is the uncertainty, A_{block} is the cross-sectional area of the heat flux block, and A_{ch} is the surface area of the segment of test section channel using four-sided cooling.

The temperature gradient uncertainty in the blocks used to measure heat flux was calculated using the equation presented in Kedzierski and Worthington [39] as the following

$$\omega_{\frac{dT}{dy}} = \sqrt{\omega_T^2 + \left(\frac{q''_{block} D_{tc}}{6 k_{cu}}\right)^2} \sqrt{\frac{1}{\sum_{i=1}^{N} (y_i - \bar{y})^2}} \tag{18}$$

where D_{tc} is the thermocouple hole diameter, k_{cu} is the thermal conductivity of copper, y_i is the vertical location of each thermocouple location used in the heat flux calculation, and $\bar{y}$ is the average thermocouple location. Sensor measurement uncertainties are summarized in Table 3. The uncertainty of all machined part lengths is half on the finest reading of the calipers used to measure the distances, corresponding to 0.005 mm. The uncertainty of the absolute pressure transducers was 0.25% full scale, corresponding to 0.75 psi (5.17 kPa). The uncertainty of the differential pressure transducer was also 0.25% full scale, corresponding to 0.075 psi (0.517 kPa). The variance in pressure drops measured was investigated. The standard deviation of the pressure drop measurements for R134a, R513A, and R450A ranged between 0.011 psi (0.076 kPa) and 0.078 psi (0.538 kPa), and the higher standard deviations corresponded to higher mass fluxes. For the lower mass fluxes (i.e., 200 and 350 kg/m^{2}s), the pressure drop uncertainty is the larger measurement error; at the highest mass flux, the standard deviation is higher than the measurement uncertainty in some cases, but typically similar to the measurement uncertainty. The uncertainty of the calibrated type T thermocouples was 0.2 °C. The wall

Table 3
Sensor measurement uncertainties

Sensor	Uncertainty
Type T thermocouples	0.2°C
Absolute pressure transducers	0.75 psi (5.17 kPa)
Differential pressure tranducers	0.075 psi (0.517 kPa)
Rotameter	R134a: 0.0858 g/s R513A: 0.0888 g/s R450A: 0.0897 g/s

temperature was extrapolated so the uncertainty of the wall temperature was calculated using

$$\omega_{T_{wall}} = \sqrt{\omega_T^2 + \left(y\omega_{\frac{dT}{dy}}\right)^2} \tag{19}$$

where the y is the distance from the bottom of the test section to the thermocouple hole (i.e., 3 mm). The fluid temperature uncertainty is based on the saturation pressure for R134a and R513A and saturation pressure and quality for R450A. For the mass flux, the uncertainty of the rotameter is 2% full scale, which corresponds to 0.0858 g/s for R134a, 0.0888 g/s for R513A, and 0.0897 g/s for R450A. The heat transfer coefficient uncertainties for all experiments were ± 6.3 – 21.2%, with an average of ± 9.8%. The heat transfer coefficient uncertainties of R134a were ± 6.3 – 10.8%, with an average of ± 7.8%. The heat transfer coefficient uncertainties of R513A were ± 8.9 – 21.2%, with an average of ± 11.8%. The heat transfer coefficient uncertainties of R450A were ± 8.0 – 12.1%, with an average of ± 9.6%.

The uncertainty of quality is calculated from the energy balances used to calculate the enthalpies. The quality uncertainty is calculated as

$$\omega_x = \sqrt{\left(\frac{\partial x}{\partial i_2}\right)^2 \omega_{i_2}^2 + \left(\frac{\partial x}{\partial i_l}\right)^2 \omega_{i_l}^2 + \left(\frac{\partial x}{\partial i_{lv}}\right)^2 \omega_{i_{lv}}^2} \tag{20}$$

where i_2 is the enthalpy in the middle of the second test section segment, i_L is the saturated liquid enthalpy and i_{lv} is the latent heat of vaporization. The uncertainty of i_2 is calculated as

$$\omega_{i_2} = \sqrt{\begin{array}{l}\left(\frac{\partial i_2}{\partial i_{pre}}\right)^2 \omega_{i_{pre}}^2 + \left(\frac{\partial i_2}{\partial \dot{Q}_{pre}}\right)^2 \omega_{\dot{Q}_{pre}}^2 + \left(\frac{\partial i_2}{\partial \dot{Q}_{header,in}}\right)^2 \omega_{\dot{Q}_{header,in}}^2 \\ + \left(\frac{\partial i_2}{\partial \dot{Q}_1}\right)^2 \omega_{\dot{Q}_1}^2 + \left(\frac{\partial i_2}{\partial \dot{Q}_2}\right)^2 \omega_{\dot{Q}_2}^2 + \left(\frac{\partial i_2}{\partial \dot{m}_{ref}}\right)^2 \omega_{\dot{m}_{ref}}^2\end{array}} \tag{21}$$

where $\dot{Q}_1$ and $\dot{Q}_2$ are the heat transfer through the first two block segments.

3. Results and Discussion

R134a, R513A, and R450A experimental condensation heat transfer coefficient results are presented. A single-phase validation was conducted using energy balances and single-phase Nusselt number correlations. The condensation heat transfer coefficient results are presented for R134a, R513A and R450A for three mass fluxes (i.e., 200, 350, and 500 kg/m^{2}s) for a quality range between 0.2 and 0.8. The mass fluxes selected covered the minimum and maximum capabilities of the compressor. Flow condensation data are compared to three condensation heat transfer correlations.

3.1. Single-phase validation

R134a, R513A, and R450A single-phase energy balances are presented in Fig. 3. The energy balance in the test section was between the heat transfer through the cooling block and the heat transfer leaving the refrigerant. The energy balance shows excellent agreement between the two heat transfer rates, calculated by Eqs. (1) and (2), well within single phase uncertainties. The deviation in the energy balances in Fig. 3 are largely due to the sensor uncertainties in measuring single-phase cooling. The refrigerant-side energy balance relies on two thermocouples for calculations, where the block-side energy balance relies on 15 thermocouples for calculations.

Fig. 4 shows the single-phase Nusselt number for R134a, R513A, and R450A. The refrigerants were compared to single-phase Nusselt number correlations. The data points within the laminar region were predicted using the Wibulswas [40] correlation, and

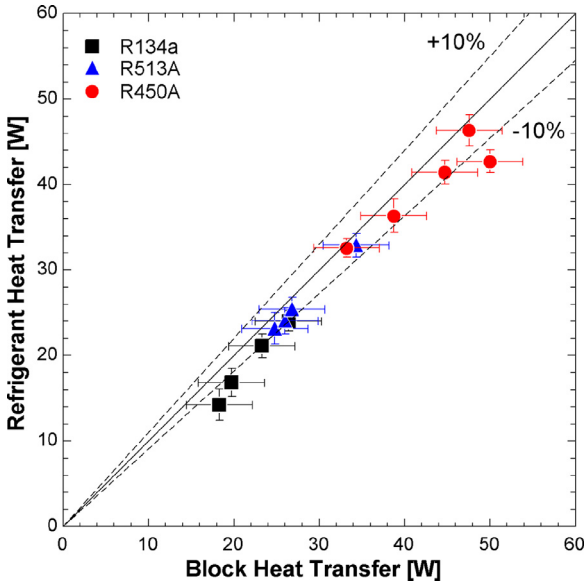

Fig. 3. Single-phase energy balances of R134a, R513A, and R450A.

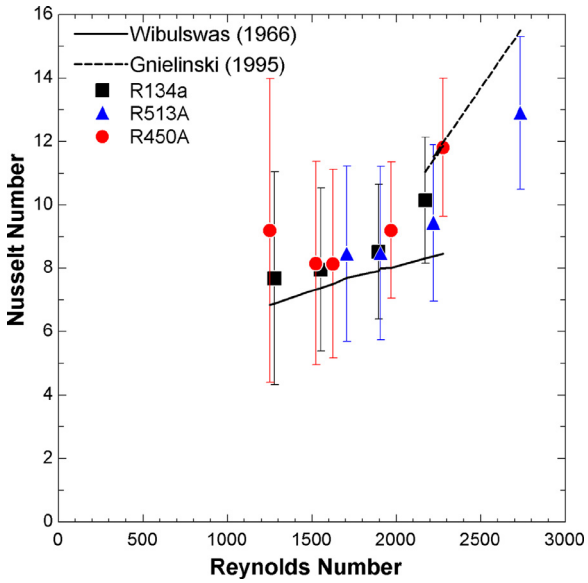

Fig. 4. Single-phase Nusselt numbers of R134a, R513A, and R450A compared to single phase correlations.

the data points within the transition region (i.e., Re>2000) were predicted using the Gnielinski [41] correlation. The Nusselt numbers showed good agreement to the correlations. The correlations are well within the uncertainties of the single-phase experiments. The higher uncertainties of the single-phase experiments and the added variability of the transition regime add to the higher variation of the Gnielinski [41] correlation predictions. The energy balances and Nusselt numbers successfully validated the data collection process.

3.2. Condensation heat transfer coefficients

Figs. 5a, b, and c show R134a, R513A, and R450A condensation transfer coefficients at mass fluxes of 200, 350, and 500 kg/m^{2}s, respectively. All data were collected at a saturation temperature of 40°C ± 1°C. The saturation temperature was a function of the saturation pressure for R134a and R513A and a function of saturation pressure and quality for R450A due to its temperature glide. Over-

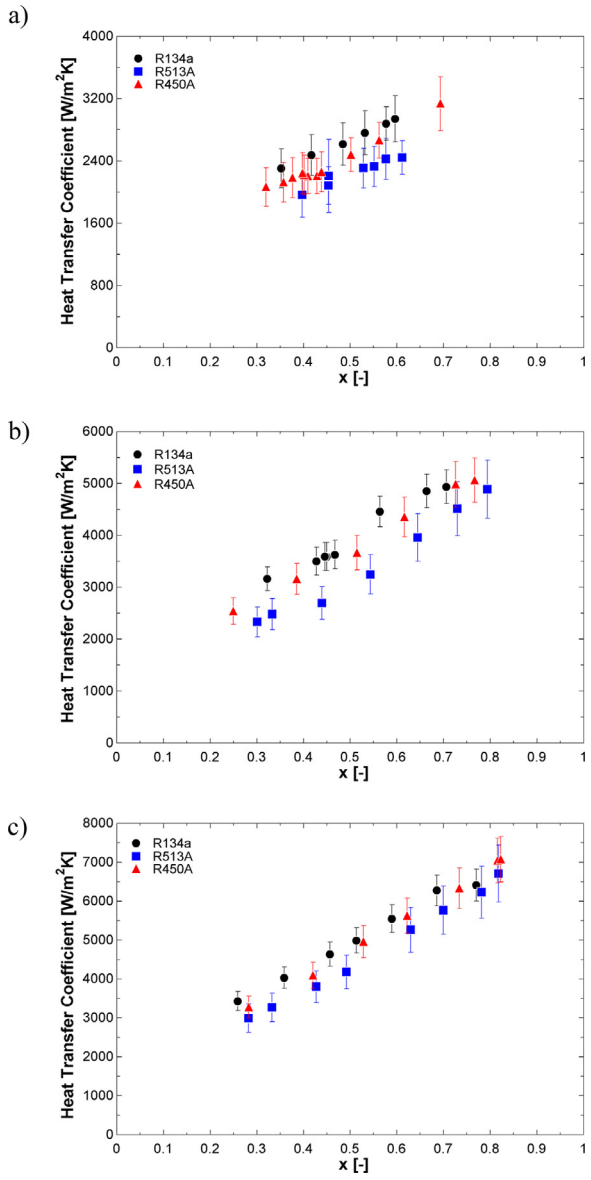

Fig. 5. Condensation heat transfer coefficients versus quality for R134a, R513A, and R450A at mass fluxes of a) 200, b) 350, and c) 500 kg/m^{2}s and a temperature of 40°C.

all, condensation heat transfer coefficients increase with increasing mass flux and quality. Increasing mass flux also increases the slope of the heat transfer coefficients for all three refrigerants with the highest slope corresponding to the higher mass flux.

R134a condensation heat transfer coefficients were generally higher than R513A and R450A in all three mass fluxes. This is consistent with most of the data in literature for R513A [28–31] and R450A [33,34]. One reason for the lower heat transfer performance of R513A is the lower liquid thermal conductivity, lower latent heat of vaporization, and higher vapor density compared to R134a. The lower thermal conductivity creates a lower conductive effect through liquid phase, and the higher vapor density creates lower velocities for a lower convective effect. The lower performance of R450A can be explained by lower thermal conductivity, lower latent heat of vaporization, and lower specific heat compared to R134a. All three properties make it more difficult for R450A to carry and conduct heat.

Direct comparison between the three refrigerants can be challenging since qualities can vary. As a result, a regression line was

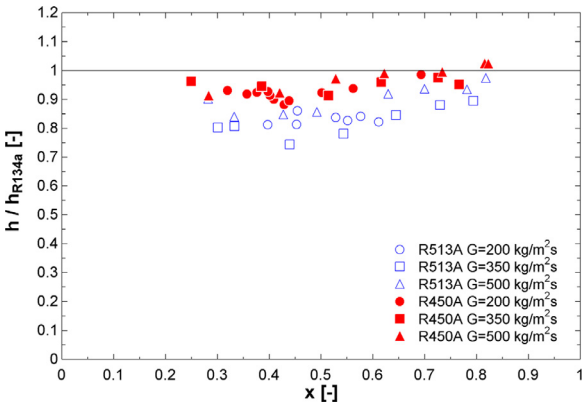

Fig. 6. Comparison of R513A and R450A to R134a heat transfer coefficients for mass fluxes of 200, 350, and 500 kg/m^{2}s.

created from the R134a data for each mass flux. R134a heat transfer coefficients were calculated using the regression line, and the R513A and R450A experimental data were compared to the calculated R134a value. The R^2 values for the R134a heat transfer coefficient curve fit equations are 0.997 (G=200 kg/m^{2}s), 0.968 (G=350 kg/m^{2}s), and 0.989 (G=500 kg/m^{2}s).

Fig. 6 presented the comparison for both R513A and R450A for all three mass fluxes. For a mass flux of 200 kg/m^{2}s, R513A showed heat transfer coefficients on average 17% (13.9 – 18.7%) less than R134a while the R450A data point at a quality of 0.69 was 1.4% lower than R134a, but the rest of the data was on average 8% (6.2 – 11.7%) lower than R134a. At a mass flux of 350 kg/m^{2}s, the R513A condensation heat transfer coefficient at a quality of 0.79 was 10.5% lower and trending away from R134a values at lower qualities to 25.6% lower at a quality of 0.44. R513A heat transfer coefficients below a quality of 0.4 were 19.2 – 19.7% lower than R134a. R450A heat transfer coefficients were on average 4.9% (2.4 – 8.7%) lower than R134a at mass flux of 350 kg/m^{2}s, with the biggest differences around a quality of 0.5. At the mass flux of 500 kg/m^{2}s, R513A heat transfer coefficients were on average 9.9% lower than R134a ranging from 2.6 to 16% lower at qualities of 0.82 and 0.28, respectively. R450A heat transfer coefficients were 2.4% lower on average than R134a with heat transfer coefficients that were 8.8% lower at low quality (i.e., 0.28) and heat transfer coefficients up to 2% higher than R134a at high quality (i.e., 0.82). Based on this analysis, R513A heat transfer coefficients were on average 15% lower than R134a; R450A heat transfer coefficients were typically 5% lower than R134a. The uncertainties of these refrigerants were large enough that it does affect the comparison between R134a, R513A, and R450A. the differences between R134a and R513A were large enough that R513A does show lower performance; however, the differences between R134a and R450A were typically around 5%, less than the average uncertainties of R450A (i.e., 9.6%).

3.3. Comparisons with condensation correlations

R134a, R513A, and R450A condensation heat transfer coefficients were compared to three condensation correlations: Kim and Mudawar [42], Shah [43], and Cavallini et al. [44]. As shown in Figs. 7a, b, and c, all three correlations tended to modestly overpredict the data. Fig. 7a presents the experimental heat transfer coefficients versus the heat transfer coefficients predicted by the Kim and Mudawar [42] correlation. The correlation shows good agreement with the experimental results with an overall mean average error (MAE) of 15.9%. The Kim and Mudawar [42] correlation predicted R134a the best; R450A had the largest MAE at 20%. Fig. 7b

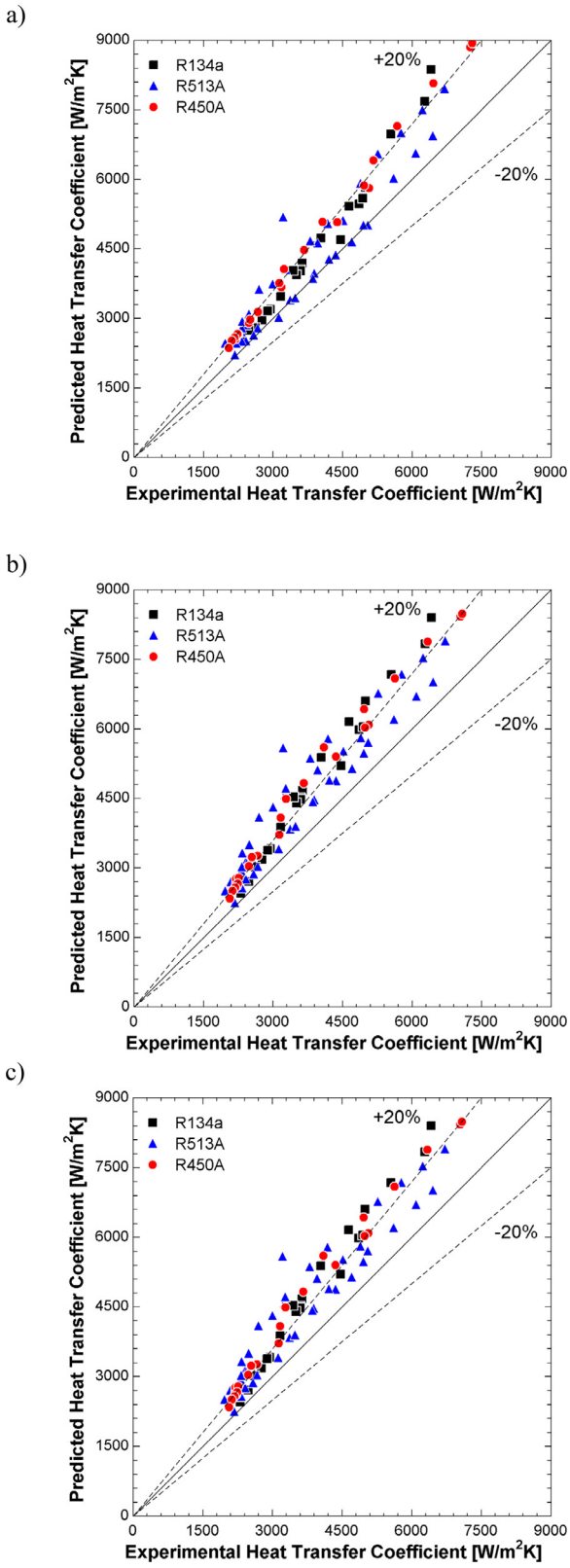

Fig. 7. Experimental condensation heat transfer coefficients versus heat transfer coefficients predicted by the a) Kim and Mudawar [42], b) Shah [43], and c) Cavallini et al. [44] correlations.

presents the experimental heat transfer coefficients versus the heat transfer coefficients predicted by the Shah [43] correlation. The Shah [43] correlation also shows good agreement with the results with an overall MAE of 23.7%. The Shah [43] correlation predicts all three refrigerants similarly. The Cavallini et al. [44] correlation predicted the data with an overall MAE of 23.7% as shown in Fig. 11. The Cavallini et al. [44] MAE is the same as the Shah MAE because Shah incorporated the equation used by Cavallini et al. [45] for Regime 1; all the experimental data collected fell into Regime 1 of the Shah [43] correlation. All three correlations predicted R134a the best as expected since they were all developed with R134a. R513A and R450A were not used in development of any of these correlations. R513A was predicted slightly better than R450A, likely due to its azeotropic nature. R450A had the highest MAEs for all three correlations, possibly due to its zeotropic nature and more complex condensing profile.

3.4. Condensation pressure drops

Condensation pressure drops are presented for R134a, R513A, and R450A at the same mass fluxes as the condensation heat transfer coefficients. Figs. 8a, b, and c present the pressure drop

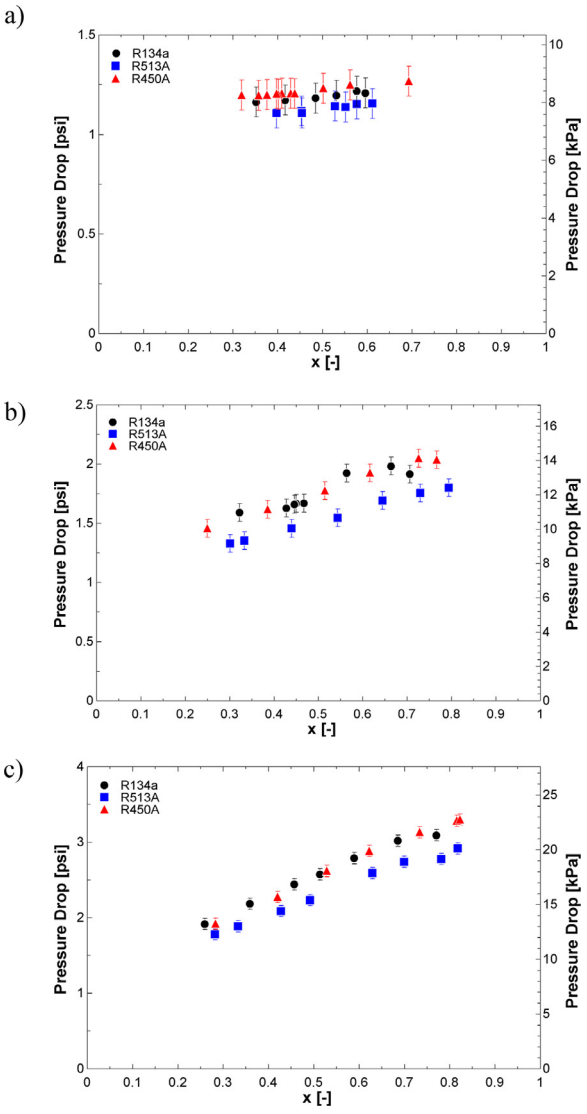

Fig. 8. Pressure drop versus quality for R134a, R513A, and R450A at a mass flux of a) 200, b) 350, and c) 500 kg/m^{2}s.

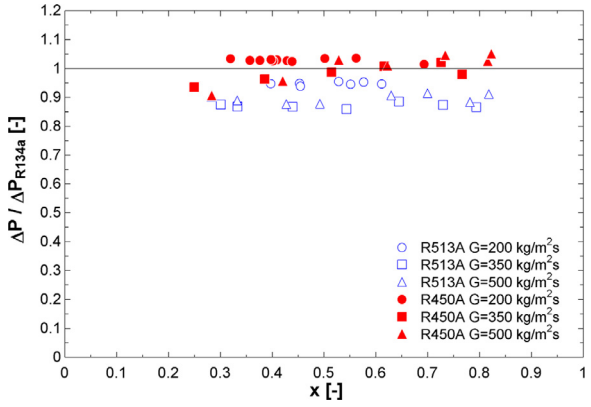

Fig. 9. Comparison of R513A and R450A to R134a pressure drop for mass fluxes of 200, 350, and 500 kg/m^{2}s.

versus quality for each mass flux. The pressure drop measurement presented includes the two cross fittings, two elbow fittings and two NPT fittings, as discussed Section 2. Pressure drop increases with increasing mass flux and quality for R134a, R513A and R450A. At a mass flux of 200 kg/m^{2}s, R513A pressure drops were about 5% lower than R134a; R450A pressure drops were marginally higher (i.e., less than 5%) than R134a. For a mass flux of 350 kg/m^{2}s, R513A pressure drops were about 10% lower than R134a while R450A pressure drops were comparable to R134a. At the highest mass flux (i.e., 500 kg/m^{2}s), R513A pressure drops were between 5 – 10% different with larger differences at high mass flux. R450A pressure drops were again comparable to R134a.

As with the comparison done for heat transfer coefficients, a curve fit equation was calculated from the R134a pressure drop data. The R^2 values for the R134a pressure drop curves are 0.941 (G=200 kg/m^{2}s), 0.862 (G=350 kg/m^{2}s), and 0.996 (G=500 kg/m^{2}s). The equation was used to compare the pressure drops of R513A and R450A to R134a pressure drops. Fig. 9 presented the comparisons between both R513A and R450A for all three mass fluxes. At a mass flux of 200 kg/m^{2}s, R513A pressure drops were on average 5.2% lower (4.5 – 6.1%) than R134a while R450A pressure drops were on average 3.0% higher (2.5 – 3.7%) than R134a. For a mass flux of 350 kg/m^{2}s, R513A pressure drops were on average 12.9% lower than R134a with minimal variation (i.e., 11.5 – 14.0%); R450A pressure drops averaged 1.8% lower than R134a, but the pressure drops ranged between 6.5% lower than R134a at a quality of 0.25 and 2.1% higher at a quality of 0.87. For a mass flux of 500 kg/m^{2}s, R513A pressure drops were on average 10.5% lower (8.6 – 12.3%) than R134a pressure drops. R450A pressure drops were on average 0.2% lower than R134a pressure drops; however, the pressure drops differences ranged from 9.5% lower at a quality of 0.28 to 5.0% higher at a quality of 0.82. R513A pressure drops are much less effected by quality than R450A which shows lower pressure drop than R134a at low quality, but higher pressure drops at high quality. This is likely due to the R1234ze(E) component of R450A, which has been shown to have higher pressure drop than R134a at high mass flux and quality [46]. R1234ze(E) and R450A do have lower vapor densities than R134a, leading to higher vapor velocities. The higher velocities cause higher pressure drops for R450A than R134a. The lower pressure drop of R513A is likely due to the R1234yf component of R513A, which has been shown to have lower condensation pressure drop than R134a [47]. The vapor densities of R1234yf and R513A are higher than R134a, leading to lower vapor velocities. The lower velocities cause lower pressure drops for R513A than R134a.

4. Conclusions

A vapor compression cycle was built to measure flow condensation heat transfer coefficients of R134a and its A1, lower global warming potential alternatives R513A and R450A. Condensation heat transfer coefficients were presented in seven 0.95-mm diameter channels at mass fluxes of 200 – 500 kg/m^{2}s, qualities between 0.2 – 0.8, and a saturation temperature of 40°C. The major conclusions for R513A are:

- R513A heat transfer coefficients were on average 14.8% lower than R134a heat transfer coefficients for all mass fluxes and qualities, ranging from 2.6% to 25.6% lower.
- At low mass flux (i.e., 200 kg/m^{2}s), the differences were consistently between 13.9% and 18.7% across the quality range (i.e., 0.40 – 0.61).
- At a mass flux of 350 kg/m^{2}s, the differences ranged from 10.5 – 25.6% with the smallest difference at high quality (i.e., 0.79) and the larger differences were at qualities below 0.6.
- At the highest mass flux (i.e., 500 kg/m^{2}s), the differences ranged from 2.6 – 16.5% with the smallest difference at the highest quality (i.e., 0.82) and the biggest difference at the lowest quality (i.e., 0.28).
- R513A heat transfer coefficients showed greater differences at lower mass fluxes and qualities and trended toward performance similar to R134a at high mass flux (i.e., 500 kg/m^{2}s) and qualities.

The major conclusions for R450A are:

- R450A heat transfer coefficients were on average 5.5% lower than R134a heat transfer coefficients were all mass fluxes and qualities, ranging from 2.4% higher to 11.7% lower than R134a.
- At a mass flux of 200 kg/m^{2}s, the differences ranged between 1.4 – 11.7% lower than R134a with the smallest difference at the highest quality (i.e., 0.69).
- At a mass flux of 350 kg/m^{2}s, the differences ranged between 2.4 – 8.7% lower than R134a.
- At the highest mass flux (i.e., 500 kg/m^{2}s), the differences ranged between 8.8% lower to 2.4% higher than R134a. The biggest lower difference was at the lowest quality (i.e., 0.28), and the biggest higher difference was at the highest quality (i.e., 0.82).

Three existing correlations were compared to the new experimental data and predicted the data fairly well. Kim and Mudawar [42] had a mean average error of 15.9%, while Shah [43] and Cavallini et al. [44] had a mean average error of 26.2%. All correlations predicted R134a the best, followed by R513A then R450A. The temperature glide of R450A likely made its prediction more difficult.

Disclosure statement

The authors report there are no competing interests to declare.

Declaration of Competing Interest

The authors have no conflict of interest to report.

CRediT authorship contribution statement

Jordan A. Morrow: Conceptualization, Methodology, Formal analysis, Investigation, Validation, Writing – original draft. **Melanie M. Derby:** Funding acquisition, Conceptualization, Methodology, Supervision, Writing – review & editing.

Acknowledgements

We would like to thank Josh Meurer for his assistance collecting experimental data. This work was supported by the National Science Foundation, Arlington, VA [grant 1828571].

Supplementary materials

Supplementary material associated with this article can be found, in the online version, at doi:10.1016/j.ijheatmasstransfer.2022.122894.

References

[1] J.M. Calm, The next generation of refrigerants–Historical review, considerations, and outlook, Int. J. Refrig. 31 (7) (2008) 1123–1133.
[2] A. Mota-Babiloni, P. Makhnatch, R. Khodabandeh, Recent investigations in HFCs substitution with lower GWP synthetic alternatives: Focus on energetic performance and environmental impact, Int. J. Refrig. 82 (2017) 288–301.
[3] G. Righetti, C. Zilio, S. Mancin, G.A. Longo, A review on in-tube two-phase heat transfer of hydro-fluoro-olefines refrigerants, Sci. Technol. Built Environ. 22 (8) (2016) 1191–1225.
[4] B. Bolaji, Z. Huan, Ozone depletion and global warming: case for the use of natural refrigerant–a review, Renewable Sustainable Energy Rev. 18 (2013) 49–54.
[5] A. Sethi, E.V. Becerra, S.Y. Motta, Low GWP R134a replacements for small refrigeration (plug-in) applications, Int. J. Refrig. 66 (2016) 64–72.
[6] A. Miyara, Condensation of hydrocarbons–A review, Int. J. Refrig. 31 (4) (2008) 621–632.
[7] A. Mota-Babiloni, J. Navarro-Esbrí, F. Molés, Á.B. Cervera, B. Peris, G. Verdú, A review of refrigerant R1234ze (E) recent investigations, Appl. Therm. Eng. 95 (2016) 211–222.
[8] A. Cavallini, D. Del Col, L. Rossetto, Heat transfer and pressure drop of natural refrigerants in minichannels (low charge equipment), Int. J. Refrig. 36 (2) (2013) 287–300.
[9] Y.-Y. Yan, T.-F. Lin, Condensation heat transfer and pressure drop of refrigerant R-134a in a small pipe, Int. J. Heat Mass Transfer 42 (4) (1999) 697–708.
[10] M. Azzolin, A. Berto, S. Bortolin, L. Moro, D. Del Col, Condensation of ternary low GWP zeotropic mixtures inside channels, Int. J. Refrig. 103 (2019) 77–90.
[11] A. Agarwal, T.M. Bandhauer, S. Garimella, Measurement and modeling of condensation heat transfer in non-circular microchannels, Int. J. Refrig. 33 (6) (2010) 1169–1179.
[12] J.A. Morrow, R.A. Huber, K. Nawaz, M.M. Derby, Flow condensation heat transfer performance of natural and emerging synthetic refrigerants, Int. J. Refrig. (2021).
[13] Y. Du, Investigation of performance of low GWP alternative to R134a in centrifugal chiller, J. Eng. Thermophys. 30 (1) (2021) 103–121.
[14] L.P.M. Colombo, A. Lucchini, L. Molinaroli, Analisi sperimentale della sostituzione del R134a con R1234yf, R1234ze (E), R450A e R513A in una pompa di calore acqua-acqua di piccola taglia (2019).
[15] Z. Meng, Y. Liu, D. Wang, L. Gao, J. Yan, Refrigerating fluid with a low global warming potential for automotive air conditioning systems in summer, Thermal Sci. (2021) (00)45-45.
[16] L. Sjoholm, Y.C. Ma, A Study of Low GWP Refrigerants for Transport Refrigeration based on Hermetic Scroll Compressors with an Economizer (2018).
[17] P. Makhnatch, A. Mota-Babiloni, A. López-Belchí, R. Khodabandeh, R450A and R513A as lower GWP mixtures for high ambient temperature countries: Experimental comparison with R134a, Energy 166 (2019) 223–235.
[18] K. Schultz, S. Kujak, System drop-in tests of R134a alternative refrigerants (ARM-42a, N-13a, N-13b, R-1234ze (E), and OpteonTM XP10) in a 230-RT water-cooled water chiller, Air-Conditioning, Heating, and Refrigeration Institute (AHRI) Low-GWP Alternative Refrigerants Evaluation Program (Low-GWP AREP),(Ed.), (2013).
[19] K. Kontomaris, J.P. Kauffman, S. Kulankara, A Reduced GWP Replacement for HFC-134a in Centrifugal Chillers: XP10 Measured Performance and Projected Climate Impact (2012).
[20] J. Sun, W. Li, B. Cui, Energy and exergy analyses of R513a as a R134a drop-in replacement in a vapor compression refrigeration system, Int. J. Refrig. 112 (2020) 348–356.
[21] P. Pardo, M. Mondot, Experimental evaluation of R410A, R407C and R134a alternative refrigerants in residential heat pumps (2018).
[22] Y.G. Saadoon, I.M. Aljubury, Experimental analysis of mobile air conditioning system using R513A as alternative refrigerants to R134a.
[23] A. Yıldız, R. Yıldırım, Investigation of using R134a, R1234yf and R513A as refrigerant in a heat pump, Int. J. Environ. Sci. Technol. 18 (5) (2021) 1201–1210.
[24] A. Mota-Babiloni, J. Navarro-Esbrí, Á. Barragán-Cervera, F. Molés, B. Peris, Drop-in analysis of an internal heat exchanger in a vapour compression system using R1234ze (E) and R450A as alternatives for R134a, Energy 90 (2015) 1636–1644.
[25] P. Makhnatch, A. Mota-Babiloni, R. Khodabandeh, Experimental study of R450A drop-in performance in an R134a small capacity refrigeration unit, Int. J. Refrig. 84 (2017) 26–35.
[26] D. Shapiro, Drop-in testing of next-generation R134a alternates in a commercial bottle cooler/freezer (2012).
[27] M. John, C. Kimambo, T.M. Eikevik, O. Nydal, J. Kihedu, Potential application of commercial refrigerants as adsorbate in adsorption refrigeration system, ISES Solar World Congress, 2017.
[28] A. López-Belchí, Assessment of a mini-channel condenser at high ambient temperatures based on experimental measurements working with R134a, R513A and R1234yf, Appl. Therm. Eng. 155 (2019) 341–353.
[29] J.A. Morrow, J. Booth, M. Derby, Comparison of mini-channel condensation heat transfer for R513A and R134a, 17th International Refrigeration and Air Conditioning Conference, Purdue University, 2018.
[30] A. Diani, L. Rossetto, Condensation of an azeotropic mixture inside 2.5 mm ID minitubes, Fluids 5 (4) (2020) 171.
[31] A. Diani, P. Brunello, L. Rossetto, R513A condensation heat transfer inside tubes: Microfin tube vs. smooth tube, Int. J. Heat Mass Transfer 152 (2020) 119472.
[32] A. Karageorgis, G. Hinopoulos, M.-H. Kim, A Comparative study on the condensation heat transfer of R-513A as an alternative to R-134a, Machines 9 (6) (2021) 114.
[33] T.A. Jacob, E.P. Matty, B.M. Fronk, Experimental investigation of in-tube condensation of low GWP refrigerant R450A using a fiber optic distributed temperature sensor, Int. J. Refrig. 103 (2019) 274–286.
[34] Y. Liu, J. Wen, P. Xu, M. Khan, S. Wang, J. Tu, Numerical investigation on the condensation of R134a, R1234ze (E) and R450A in mini-channels, Int. J. Refrig. (2021).
[35] M.M. Derby, A. Chatterjee, Y. Peles, M.K. Jensen, Flow condensation heat transfer enhancement in a mini-channel with hydrophobic and hydrophilic patterns, Int. J. Heat Mass Transfer 68 (2014) 151–160.
[36] M. Derby, H.J. Lee, Y. Peles, M.K. Jensen, Condensation heat transfer in square, triangular, and semi-circular mini-channels, Int. J. Heat Mass Transfer 55 (1-3) (2012) 187–197.
[37] M.M. Derby, Study of Flow Condensation Enhancement with Hydrophobic and Hydrophilic Patterns, Rensselaer Polytechnic Institute, 2013.
[38] S.J. Kline, F.A. McClintock, Describing uncertainty in single sample experiments, ASME Mech Eng 75 (1953) 3–8.
[39] M.A. Kedzierski, J.L. Worthington III, Design and machining of copper specimens with micro holes for accurate heat transfer measurements, Exp. Heat Transfer 6 (4) (1993) 329–344.
[40] P. Wibulswas, Laminar-Flow Heat-Transfer in Non-Circular Ducts, University of London, 1966.
[41] V. Gnielinski, A new method to calculate heat transfer in the transition region between laminar and turbulent tube flow; Ein neues Berechnungsverfahren fuer die Waermeuebertragung im Uebergangsbereich zwischen laminarer und turbulenter Rohrstroemung, Forsch. Ingenieurwes. 61 (1995).
[42] S.-M. Kim, I. Mudawar, Universal approach to predicting heat transfer coefficient for condensing mini/micro-channel flow, Int. J. Heat Mass Transfer 56 (1-2) (2013) 238–250.
[43] M.M. Shah, A correlation for heat transfer during condensation in horizontal mini/micro channels, Int. J. Refrig. 64 (2016) 187–202.
[44] A. Cavallini, S. Bortolin, D. Del Col, M. Matkovic, L. Rossetto, Condensation heat transfer and pressure losses of high-and low-pressure refrigerants flowing in a single circular minichannel, Heat Transfer Eng. 32 (2) (2011) 90–98.
[45] J.S. Brown, C. Zilio, R. Brignoli, A. Cavallini, Thermophysical properties and heat transfer and pressure drop performance potentials of hydrofluoro-olefins, hydrochlorofluoro-olefins, and their blends, HVAC&R Research 20 (2) (2014) 203–220.
[46] J. Wang, J.M. Li, Pressure drop of R134a and R1234ze (E) during condensation in horizontal microchannel arrays cooled symmetrically and asymmetrically, Exp. Therm Fluid Sci. 96 (2018) 266–283.
[47] F. Illán-Gómez, A. López-Belchí, J. García-Cascales, F. Vera-García, Experimental two-phase heat transfer coefficient and frictional pressure drop inside mini-channels during condensation with R1234yf and R134a, Int. J. Refrig. 51 (2015) 12–23.